



# Resurrection of Type IIL Supernova 2018ivc: Implications for a Binary Evolution Sequence Connecting Hydrogen-rich and Hydrogen-poor Progenitors

Keiichi Maeda<sup>1</sup> , Tomonari Michiyama<sup>2,3</sup> , Poonam Chandra<sup>4</sup> , Stuart Ryder<sup>5,6</sup> , Hanindy Kuncarayakti<sup>7,8</sup> ,  
Daichi Hiramatsu<sup>9,10,11,12</sup> , and Masatoshi Imanishi<sup>3,13</sup>

<sup>1</sup> Department of Astronomy, Kyoto University, Kitashirakawa-Oiwake-cho, Sakyo-ku, Kyoto, 606-8502, Japan; [keiichi.maeda@kustro.kyoto-u.ac.jp](mailto:keiichi.maeda@kustro.kyoto-u.ac.jp)

<sup>2</sup> Department of Earth and Space Science, Osaka University, 1-1 Machikaneyama, Toyonaka, Osaka 560-0043, Japan

<sup>3</sup> National Astronomical Observatory of Japan, National Institutes of Natural Sciences (NINS), 2-21-1 Osawa, Mitaka, Tokyo 181-8588, Japan

<sup>4</sup> National Radio Astronomy Observatory, 520 Edgemont Road, Charlottesville, VA 22903, USA

<sup>5</sup> School of Mathematical and Physical Sciences, Macquarie University, Sydney, NSW 2109, Australia

<sup>6</sup> Macquarie University Research Centre for Astronomy, Astrophysics & Astrophotonics, Sydney, NSW 2109, Australia

<sup>7</sup> Tuorla Observatory, Department of Physics and Astronomy, FI-20014 University of Turku, Finland

<sup>8</sup> Finnish Centre for Astronomy with ESO (FINCA), FI-20014 University of Turku, Finland

<sup>9</sup> Center for Astrophysics, Harvard & Smithsonian, 60 Garden Street, Cambridge, MA 02138-1516, USA

<sup>10</sup> The NSF AI Institute for Artificial Intelligence and Fundamental Interactions, USA

<sup>11</sup> Las Cumbres Observatory, 6740 Cortona Drive, Suite 102, Goleta, CA 93117-5575, USA

<sup>12</sup> Department of Physics, University of California, Santa Barbara, CA 93106-9530, USA

<sup>13</sup> Department of Astronomy, School of Science, The Graduate University for Advanced Studies, Sokendai, Mitaka, Tokyo 181-8588, Japan

Received 2022 November 9; revised 2023 January 3; accepted 2023 January 11; published 2023 March 1

## Abstract

Long-term observations of synchrotron emission from supernovae (SNe), covering more than a year after the explosion, provide a unique opportunity to study the poorly understood evolution of massive stars in the final millennium of their lives via changes in the mass-loss rate. Here we present a result of our long-term monitoring of the peculiar Type IIL SN 2018ivc using the Atacama Large Millimeter/submillimeter Array. Following the initial decay, it showed unprecedented rebrightening starting  $\sim 1$  yr after the explosion. This is one of the rare examples showing such rebrightening in the synchrotron emission and the first case at millimeter wavelengths. We find it to be in the optically thin regime, unlike the optically thick centimeter emission. As such, we can robustly reconstruct the distribution of the circumstellar matter and thus the mass-loss history in the final  $\gtrsim 1000$  yr. We find that the progenitor of SN 2018ivc had experienced a very high mass-loss rate ( $\gtrsim 10^{-3} M_{\odot} \text{ yr}^{-1}$ )  $\sim 1500$  yr before the explosion, which was followed by a moderately high mass-loss rate ( $\gtrsim 10^{-4} M_{\odot} \text{ yr}^{-1}$ ) up until the explosion. From this behavior, we suggest that SN 2018ivc represents an extreme version of a binary evolution toward SNe Ib, which bridges the hydrogen-poor SNe (toward SNe Ib/c, without a hydrogen envelope) and hydrogen-rich SNe (SNe IIP, with a massive envelope).

*Unified Astronomy Thesaurus concepts:* [Supernovae \(1668\)](#); [Circumstellar matter \(241\)](#); [Radio sources \(1358\)](#); [Non-thermal radiation sources \(1119\)](#); [Millimeter astronomy \(1061\)](#); [Stellar evolution \(1599\)](#)

## 1. Introduction

The evolution of massive stars toward core collapse and supernova (SN) explosions has not been fully understood, especially in their post-main-sequence (MS) evolution (e.g., Langer 2012; Maeda 2022). Studying the pre-SN mass-loss history through observational data after the SN explosion sheds light on this issue; it is essentially the one and only method to probe massive star evolution in the final millennium to even less than 1 yr (e.g., Smith 2017). The radio synchrotron emission, as created at the shock wave formed by the interaction between the SN ejecta and the circumstellar matter (CSM), is a direct probe to the CSM distribution (e.g., Chevalier 1998; Chevalier & Fransson 2006; Maeda 2012; Matsuoka et al. 2019). For the typical SN shock velocity of  $\sim 10,000 \text{ km s}^{-1}$  and the CSM velocity of  $\sim 20 \text{ km s}^{-1}$  (for a case of a supergiant progenitor; Smith 2017), the nature of the CSM probed by the synchrotron signal a few years after the

explosion translates to the mass-loss rate  $\sim 1000$  yr before the explosion.

The SNe Ib are a particularly interesting type of SN in this context. They are defined by the initial appearance of hydrogen lines in their optical spectra that eventually disappear (Filippenko 1997), indicating that they do not have an H-rich envelope as massive as canonical SNe II (red supergiants) while still keeping  $\sim 0.01\text{--}1 M_{\odot}$  of the envelope (e.g., Shigeyama et al. 1994; Woosley et al. 1994; Bersten et al. 2012; Hiramatsu et al. 2021), the features that distinguish SNe Ib from the more stripped envelope analogs, i.e., SNe Ib (He stars) or SNe Ic (C+O stars). As such, SNe Ib bridge SNe II and SNe Ib/c in terms of the pre-SN mass-loss mechanism, especially that responsible for ejecting the H-rich envelope (e.g., Fang et al. 2019). The binary evolution channel is a leading scenario for the envelope stripping from SNe II toward SNe Ib/Ib/Ic (e.g., Ouchi & Maeda 2017; Yoon 2017), whose progenitors probably share a similar initial mass range (e.g., Fang et al. 2019). Details are, however, yet to be clarified.

Discovered by the  $D < 40$  Mpc SN survey (Tartaglia et al. 2018) on 2018 November 24 (UT) within a day of the explosion (Valenti et al. 2018; Bostroem et al. 2020), SN 2018ivc is an outlier of the SN IIL subclass with its faint and rapidly evolving



Original content from this work may be used under the terms of the [Creative Commons Attribution 4.0 licence](#). Any further distribution of this work must maintain attribution to the author(s) and the title of the work, journal citation and DOI.

**Table 1**  
ALMA Measurements of SN 2018ivc

MJD	Phase <sup>a</sup> (days)	Frequency <sup>b</sup> (GHz)	$F_{\nu}$ <sup>c</sup> (mJy)	Array	Resolution <sup>d</sup>	ID	PI
Band 3							
58,449.1 <sup>e</sup>	4.1	100.0	$4.25 \pm 0.22$	C43-4	0''70	2018.1.01193.T	K. Maeda
58,452.1 <sup>e</sup>	7.1	100.0	$7.42 \pm 0.38$	C43-4	0''94	2018.1.01193.T	K. Maeda
58,462.1 <sup>e</sup>	17.1	100.0	$9.05 \pm 0.46$	C43-4	1''17	2018.1.01193.T	K. Maeda
58,466.0	21.0	93.5	$7.41 \pm 0.99$	C43-4	1''14	2018.1.01506.S	S. Viti
58,643.6 <sup>e</sup>	198.6	100.0	$0.336 \pm 0.026$	C43-9	0''06	2018.A.00038.S	K. Maeda
58,658.5	213.5	92.1	$0.322 \pm 0.036$	C43-9	0''05	2018.1.01135.S	J. Wang
58,751.2	306.2	103.0	$0.264 \pm 0.044$	C43-6	0''33	2018.1.01684.S	T. Tosaki
59,469.4	1024.4	92.1	$1.128 \pm 0.069$	C43-9	0''05	2019.1.00026.S	M. Imanishi
59,809.4	1364.4	100.0	$0.955 \pm 0.093$	C-5	0''76	2021.A.00026.S	K. Maeda
Band 6							
58,449.1 <sup>e</sup>	4.1	250.0	$4.21 \pm 0.43$	C43-4	0''28	2018.1.01193.T	K. Maeda
58,451.2 <sup>e</sup>	6.2	250.0	$4.32 \pm 0.44$	C43-4	0''42	2018.1.01193.T	K. Maeda
58,462.1 <sup>e</sup>	17.1	250.0	$2.49 \pm 0.28$	C43-4	0''50	2018.1.01193.T	K. Maeda
58,643.6 <sup>e</sup>	198.6	250.0	$0.120 \pm 0.022$	C43-9	0''03	2018.A.00038.S	K. Maeda
59,809.4	1364.4	250.0	$0.286 \pm 0.067$	C-5	0''30	2021.A.00026.S	K. Maeda

#### Notes.

<sup>a</sup> The phase is measured from the putative explosion date (MJD 58,445.0).

<sup>b</sup> Central frequency.

<sup>c</sup> With  $1\sigma$  error.

<sup>d</sup> Average of the major and minor axes.

<sup>e</sup> From Maeda et al. (2023).

optical light curve. Maeda et al. (2023) presented and analyzed the data taken by the Atacama Large Millimeter/submillimeter Array (ALMA) covering 4–198 days since the (well-determined) explosion date, together with the optical and X-ray light curves. They suggested that SN 2018ivc is indeed an analog of an SN I Ib explosion (potentially with a slightly more massive H-rich envelope), with its different observational features from canonical SNe I Ib originating in its powering mechanism, the SN–CSM interaction. Such a scenario may also be in line with its optical spectral features showing broad and boxy emission lines (Dessart & Hillier 2022). Maeda et al. (2023) further proposed that SN 2018ivc and a fraction of SNe IIL may be a direct link between SNe I Ib and SNe IIP in the binary evolution where the sequence of SNe Ic/Ib–I Ib–(some) IIL–IIP is mainly controlled by the initial orbital separation. This is along the same line as previously suggested by Nomoto et al. (1995, 1996) but with a substantial difference in the mode of binary interaction (see Section 4 for more details).

The proximity (8''7 east and 16''1 north) of SN 2018ivc to the core of the well-studied Seyfert galaxy NGC 1068 (M77), for which we assume a distance of  $10^{+1.8}_{-1.5}$  Mpc (Tully et al. 2009), requires a high angular resolution to resolve this SN, but at the same time it offers a unique opportunity for long-term monitoring; the SN location may be covered by archival observations targeting the core of NGC 1068. Recently, its detection at  $\sim 1000$  days after the explosion in the centimeter emission, at 6.5 GHz by the Karl G. Jansky Very Large Array (VLA), and at 6.3 GHz by the enhanced Multi-Element Radio Linked Interferometer Network was reported (Mutie et al. 2022). In this paper, we report the result of our long-term monitoring of SN 2018ivc with ALMA. The paper is structured as follows. In Section 2, we present the observation and data reduction. Results are presented in Section 3, with the analysis of the nature of the CSM at a large scale around SN 2018ivc.

Its implications for the progenitor evolution of SN 2018ivc and its relation to other classes of SNe are discussed in Section 4. The paper is summarized in Section 5 with concluding remarks.

## 2. Observations and Data Reduction

In this paper, we report late-time observations of SN 2018ivc ( $\gtrsim 1000$  days) based on data taken through ALMA Director’s Discretionary Time (DDT) program 2021.A.00026.S (PI: K. Maeda), complemented by the data at earlier epochs published in Maeda et al. (2023) and archival data newly presented in this work. The log of the data used in the present work, together with the measured fluxes, is shown in Table 1. The DDT program was conducted on 2022 August 18 (1364 days since the explosion), essentially in the same spectral setup with our early-phase observations up to  $\sim 200$  days. On-target exposure time is 5.0 minutes for band 3 and 9.6 minutes for band 6. The central frequencies in the continuum bands are 100 and 250 GHz. The angular resolution is  $0''81 \times 0''71$  in band 3 and  $0''33 \times 0''28$  in band 6 (Figure 1). Since this observation targeted the SN, i.e., the point source, the imaging processes are simple. We use the data calibrated through the standard ALMA pipeline with Common Astronomy Software Applications (CASA; The CASA Team et al. 2022). The continuum flux densities associated with the SN in each image are measured based on the `imfit` task in CASA.

In addition, we use ALMA band 3 archival data that cover the position of SN 2018ivc. We selected the data in which the SN is detected at a signal-to-noise ratio (S/N) of  $>5$ . We downloaded the processed continuum images by the Japanese Virtual Observatory. In the cases of 2018.1.01135.S and 2019.1.00026.S, we manually performed the imaging processes, i.e., the `clean` task in CASA with primary beam correction, because the archival images do not cover the SN position. For 2018.1.01135.S, we conducted standard self-

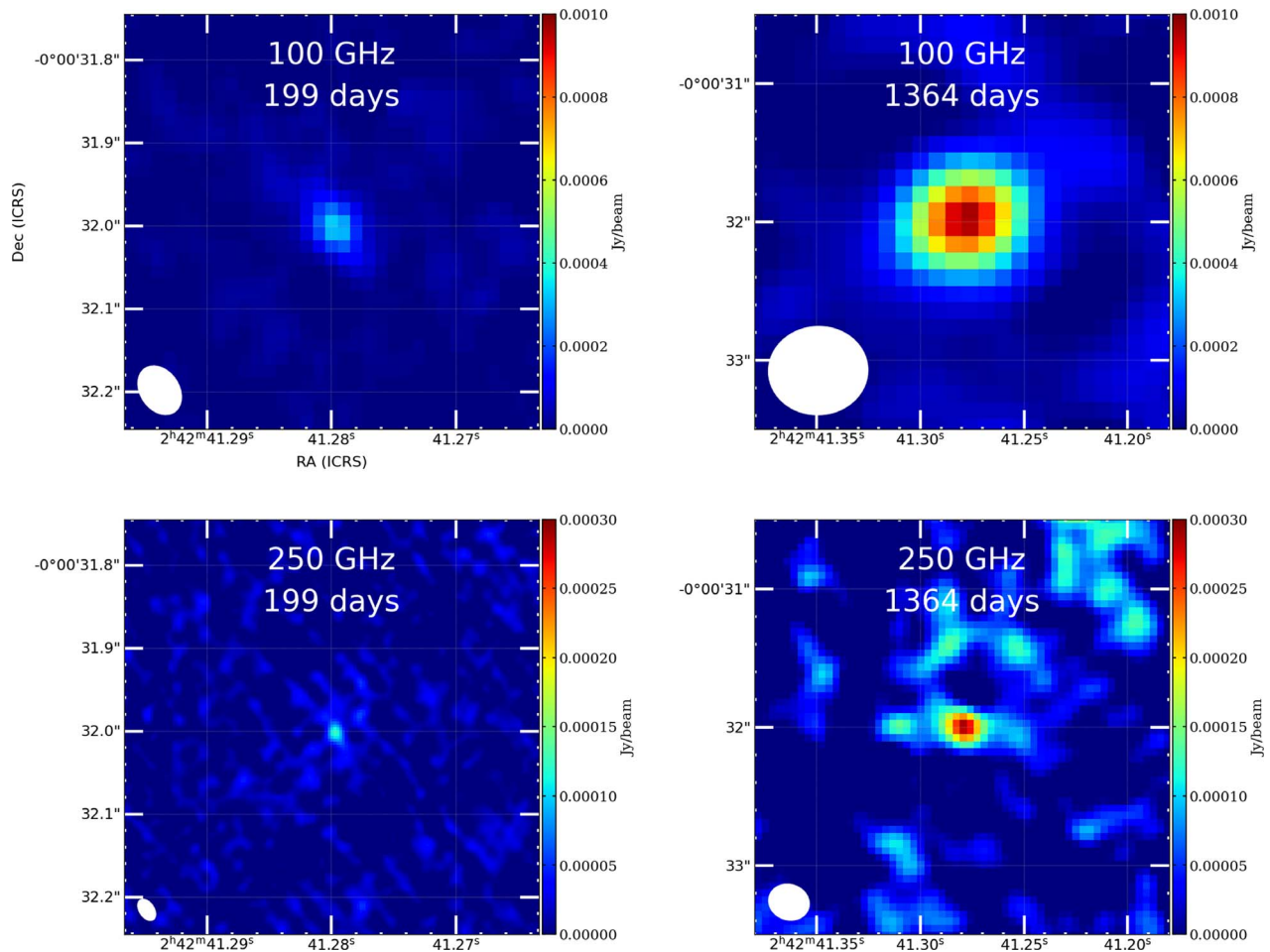


**Figure 1.** ALMA band 3 (top) and band 6 (bottom) images of SN 2018ivc on days 199 (left; Maeda et al. 2023) and 1364 (right). The elliptical beam shape is shown in the bottom left corner in each panel.

calibration to minimize the effects by side lobes from the bright nuclear emission. The S/N was improved by self-calibration, but the flux value associated with the SN is consistent regardless of the self-calibration processes. For 2019.1.00026. S, the data were taken during several visits over the course of  $\sim 2$  weeks, and we select those that provide the best S/N at the SN position.

### 3. Results

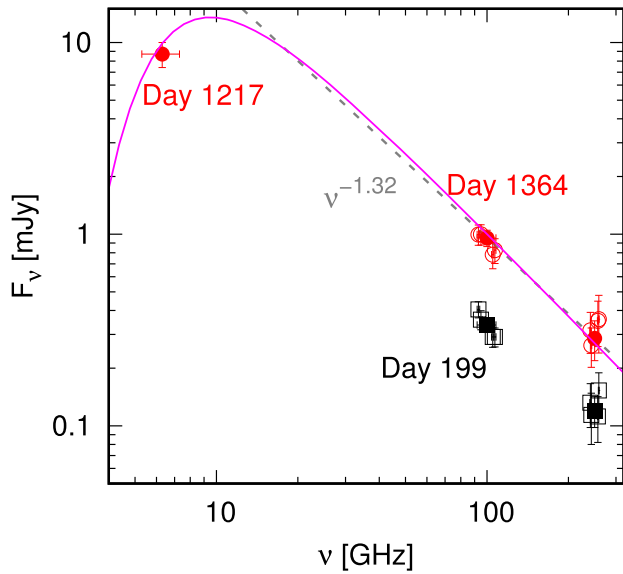
Figure 1 shows the reconstructed images of SN 2018ivc on days 199 (Maeda et al. 2023) and 1364 (this work). After the flux decay in the earlier phase up to  $\sim 200$  days, the SN has begun brightening again. There is a hint of a slow decay between days 1024 and 1364, but they are also consistent with the same flux level within  $1\sigma$  (after correcting for the central frequency difference).

Figure 2 compares the spectral energy distributions (SEDs) on days 199 and 1364, with the addition of the centimeter flux on day 1217 taken from Mutie et al. (2022). It is clear that SN 2018ivc remains optically thin in the high-frequency emission in the ALMA bands. Assuming  $f_\nu \propto \nu^\alpha$ ,  $\alpha = -1.32 \pm 0.15$  ( $1\sigma$ ) is measured on day 1364. Given the SED slope of  $\alpha = -1.12 \pm 0.22$  on day 199 (Maeda et al. 2023), there is a hint of the spectral steepening, but it is also consistent with no change within  $1\sigma$  (i.e.,  $\alpha = -1.22 \pm 0.27$  for the combined analysis of the data on days 199 and 1364). The SED as found

in our ALMA observations also indicates that the centimeter emission must be in the optically thick regime. This highlights the power of the higher-frequency observation despite the generally lower flux level; catching the optically thin portion of the synchrotron emission is essential to constrain the CSM properties (Maeda et al. 2021, 2023).

Figure 3 shows the light curves. Rebrightening at 100 and 250 GHz is clearly seen, which probably started at  $\sim 300$  days. Since it has been optically thin in the ALMA bands both before and after the rebrightening (Figure 2), the flux increase means that the CSM is not smoothly distributed, and that the CSM density in the outer region must be higher than the extrapolation from the inner region.

We have computed a series of synchrotron emission models (see Maeda et al. 2021, 2023) by considering a CSM extended outward from  $\sim 4 \times 10^{16}$  cm (i.e., with the main interaction taking place at  $\sim 500$  days for the SN ejecta velocity of  $\sim 10,000$  km s $^{-1}$ ). In practice, we simply assume that the CSM is distributed with a density structure of  $\rho_{\text{CSM}} \propto Dr^{-s}$  without a hole in the computation (where  $D = \dot{M}/4\pi v_w$ ,  $\dot{M}$  is the mass-loss rate, and  $v_w$  is the mass-loss wind velocity). Once the interaction has fully developed at  $\sim 500$  days (at  $\sim 4 \times 10^{16}$  cm), the mass of the swept-up CSM is expected to soon be dominated by the outer component; therefore, the evolution of the SN–CSM interaction will quickly lose the memory of the earlier interaction and follow the asymptotic behavior



**Figure 2.** The SED of SN 2018ivc on day  $\sim 1300$  (red circles), as constructed from the data at 6.3 (Mutie et al. 2022) and 100/250 (this work) GHz. For comparison, the SED on day 199 (black squares) is also shown (Maeda et al. 2023). The flux densities derived for the individual spectral windows (SPWs) are shown by open symbols, while the flux densities after combining the four continuum SPWs within each band are shown by filled symbols. The flux densities are shown with  $1\sigma$  errors; the flux calibration error is included for the SPW-combined data, while it is omitted for the individual SPW data. The power-law fit to the ALMA data on day 1364 is shown by the dashed line. For demonstration purposes, the SED computed for the model with  $s = 1$  is shown (magenta; see also Figure 3).

determined by the outer CSM component. We thus apply this model to the epoch after  $\sim 500$  days.

The ejecta structure and microphysics parameters are the same as those adopted by Maeda et al. (2023) for the early-phase modeling:  $M_{\text{ej}} = 3 M_{\odot}$ ,  $E_{\text{K}} = 1.2 \times 10^{51}$  erg, and the outer ejecta density slope of  $n = -10$ . The centimeter emission is in the optically thick regime, and we find that the synchrotron self-absorption alone would not explain the cutoff at the low frequency. We thus include free-free absorption, which is, however, poorly constrained by theory. We simply vary the optical depth by changing the constant electron temperature in the unshocked CSM. It is just for demonstration, and in most of the subsequent analyses, we do not use constraints from the centimeter observations due to the large uncertainty in the model framework.

Figure 3 shows models with four different CSM distributions:  $s = -2$  (i.e., increasing density), 0 (constant), 1, and 2 (steady-state mass loss). These CSM distributions are plotted in Figure 4. By changing the density scale ( $D$ ), all of the models can reproduce the flux levels at the latest epochs (1024 and 1364 days). The flat ( $s=0$ ) and increasing ( $s=-2$ ) CSM distributions are not favored, given the nearly flat or slowly decaying evolution observed during this time window. The model with  $s=1$  provides the best representation of the evolution, while our focus in the present work is the CSM density scale without aiming at constraining the value of  $s$ . It is possible to explain the flux levels at 6.5/6.3 GHz in the optically thick emission; within a simple treatment of the free-free absorption, we are, however, not able to explain the flat or slowly decaying evolution also seen in the centimeter emission. We emphasize that the centimeter emission, including both the model and the calibration of the data, is not a topic of this work.

While there is a degeneracy in the CSM slope given the limited temporal coverage, the CSM density at  $\sim 10^{17}$  cm is strongly constrained to be  $\sim 10^{-18}$  g cm $^{-3}$ ; this is where the data points exist. It is substantially above the extrapolation from the inner structure, and it is about an order of magnitude larger in terms of the mass-loss rate (assuming that  $v_w$  did not change).

#### 4. Discussion

In the SN I Ib scenario with an extended progenitor (Maeda et al. 2023), the mass-loss velocity would be  $\sim 20$  km s $^{-1}$  (e.g., Groh 2014; Smith 2017). Then, the location of the “outer” dense CSM ( $\sim 10^{17}$  cm) corresponds to the mass-loss history  $\sim 1500$  yr before the explosion. Based on the binary evolution model toward SNe I Ib (Ouchi & Maeda 2017), Maeda et al. (2023) suggested that the progenitor of SN 2018ivc might have experienced an extreme case of the case C mass transfer, where the binary mass transfer is initiated in the advanced evolution stage after the core He ignition (e.g., Langer 2012), to explain the high mass-loss rate just before the explosion as inferred from the early-phase observation (see also Maeda et al. 2015). As compared to other SNe I Ib, it is suggested that the strong binary interaction has taken place later in its evolution, closer to the time of the core-collapse explosion, which is attributed to a larger initial orbital separation.

Ouchi & Maeda (2017) indeed predicted that the extreme case C mass transfer may bridge the evolution toward SNe I Ib and SNe I IP, where the SNe are surrounded by a dense CSM will be identified as either SNe I IL or I In. In Figure 4, we show two such models showing late-time binary interaction (Ouchi & Maeda 2017) for the initial masses of the primary and secondary of 16 and 9.6  $M_{\odot}$ , with the only difference in the initial orbital period (1800 days for model 25 and 1950 days for model 28). In both models, the binary first experiences rapid mass transfer until the mass ratio is inverted, during which most of the H-rich envelope ( $\gtrsim 5 M_{\odot}$ ) is ejected. This is then followed by a relatively high mass-transfer rate of  $\gtrsim 10^{-5} M_{\odot}$  yr $^{-1}$  as the primary keeps filling the Roche lobe (RL). The final leftover envelope mass is  $\sim 2 M_{\odot}$  in these models, which is somewhat large for an SN I Ib but qualitatively consistent with the extended SN I Ib progenitor scenario with a slightly more massive envelope than canonical SNe I Ib; the final envelope mass should be dependent on the binary parameters, especially the mass ratio that roughly controls the mass of the leftover envelope after the rapid-transfer phase (see above). The initial rapid transfer takes place  $\sim 5800$  and  $\sim 300$  yr before the explosion for models 25 and 28, respectively.

While the timing is different, the mass-loss properties during the initial rapid-transfer phase are similar (Figure 4). It is thus possible, in principle, to have the strong interaction phase at  $\sim 1500$  yr where most of the envelope,  $\gtrsim 5 M_{\odot}$ , is ejected, which forms the dense CSM at  $\sim 10^{17}$  cm, by a different combination of the component masses and the initial separation. This is demonstrated in Figure 4 by comparing the mass-loss history derived for SN 2018ivc and those predicted by models 25 and 28 of Ouchi & Maeda (2017). Indeed, if we shift the mass-loss history of model 25 toward the explosion date, assuming slightly different binary parameters (e.g., the initial separation and/or initial mass ratio), it can explain that derived for SN 2018ivc reasonably well.

In optical wavelengths, SNe I Ib from “extended” progenitors tend to show signs of the SN-CSM interaction in the late phase

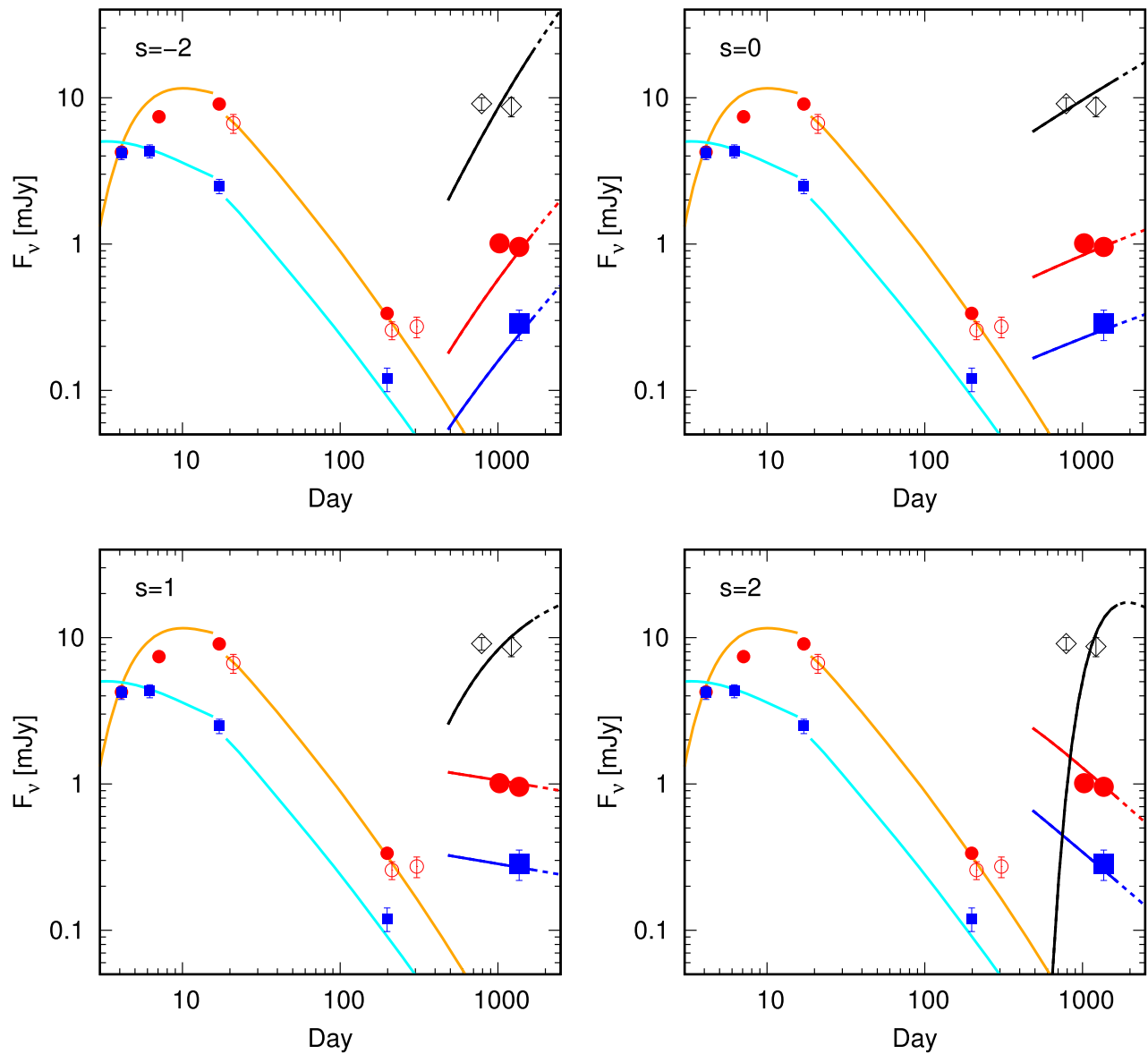


**Figure 3.** Radio light curves of SN 2018ivc. The high-frequency data are taken by ALMA at 100 (red circles) and 250 (blue squares) GHz, including the data from Maeda et al. (2023; small filled symbols), the new late-time data at  $>1000$  days (large filled symbols), and the other archival data (open symbols). The late-time centimeter flux densities at 6.3/6.5 GHz (black open diamonds) are taken from Mutie et al. (2022). For band 3 data, the flux densities are corrected to those at 100 GHz, assuming the SED slope seen in a neighboring epoch when the SN was observed in both band 3 and band 6 (see Figure 2). The model curves at 100 (orange) and 250 (cyan) GHz in the earlier phase ( $\lesssim 200$  days) are from Maeda et al. (2023). The four panels are shown with different models for the late-phase light curves at 6.5 (black), 100 (red), and 250 (blue) GHz with  $s = -2, 0, 1,$  and  $2$  for the CSM slope.

( $\gtrsim 1$  yr) as the emergence of strong  $H_{\alpha}$  emission and light-curve flattening (Patat et al. 1995; Matheson et al. 2000; Maeda et al. 2015; Fremling et al. 2019). However, it is more likely that the late-time emergence of the SN–CSM interaction in these cases is simply due to the decreasing importance of other powering mechanisms (e.g.,  $^{56}\text{Ni}/\text{Co}$  decay), and it would not require an increase of the SN–CSM interaction power by a distinct high-density CSM component (Maeda et al. 2015). It is naturally expected if the timing of the strong binary interaction occurred earlier for these systems than for SN 2018ivc; in this case, the CSM created by the first rapid mass-transfer phase must be located far outside.

To our knowledge, this is the second SN I Ib for which a clear radio rebrightening has been detected; the first example is the somewhat peculiar SN I Ib 2003bg, suggested to be a broad-lined SN I Ib (Hamuy et al. 2009) that showed a jump in the

radio flux by a factor of 2 or 3 at  $\sim 100$  days (Soderberg et al. 2006). We also note that SN I Ib 2001ig showed a modulation superimposed on a long-term decline in its radio light curves (Ryder et al. 2004). These SNe I Ib may share some common evolutionary path to SN 2018ivc. Possible modulations were also seen in SN I Ib 2004C (DeMarchi et al. 2022), though the sparse sampling at such late times makes it hard to ascertain their magnitude and timescale. In any event, SN 2004C did not show a sustained transition from decay to rebrightening. It is nevertheless one of the only two SNe I Ib included in the sample of late-time radio monitoring by Stroh et al. (2021), with the other example lacking information on its temporal evolution.

Radio rebrightening is rare for SNe, and only a handful of events are known so far (e.g., Bauer et al. 2008). Of particular interest are a few SNe I b/c showing a transition to SNe I In and

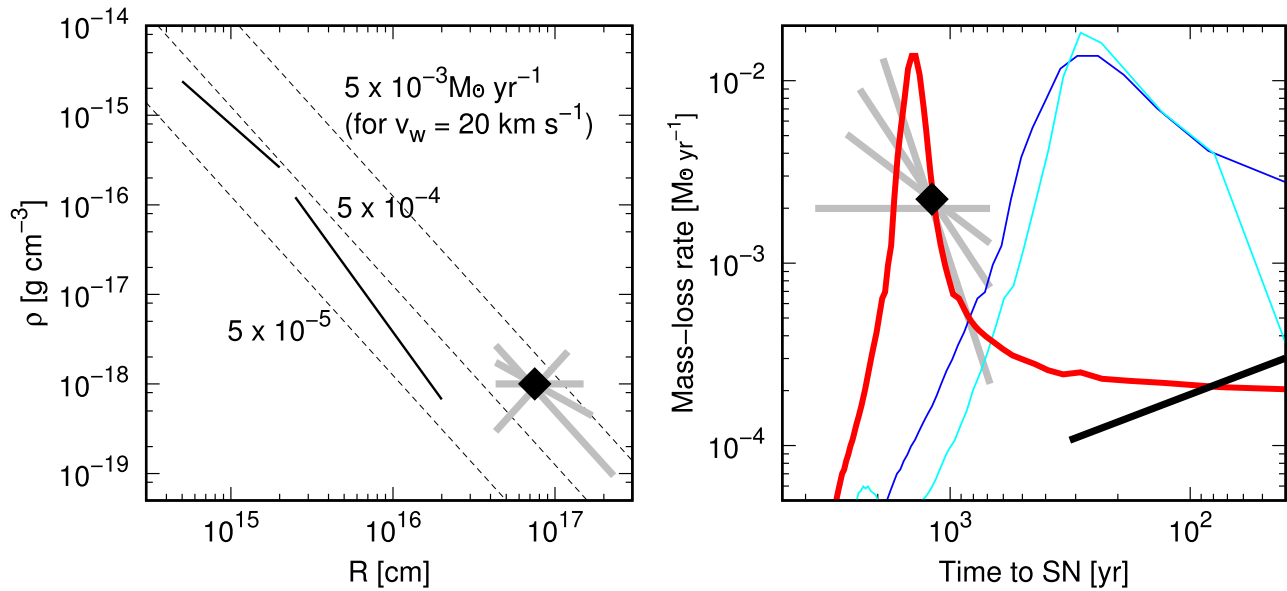


**Figure 4.** Left: CSM distribution derived for SN 2018ivc. The inner structure at  $\lesssim 2 \times 10^{16}$  cm (black lines) is from Maeda et al. (2023). The CSM distributions adopted in the light-curve models ( $s = -2, 0, 1,$  and  $2$ ) for the late epochs (Figure 3) are shown by the gray lines, where the overlapping region (black diamond) is strongly constrained irrespective of the model details. Right: mass-loss history toward the SN (black line and point for SN 2018ivc). The mass-loss histories based on models 25 (peak at 5800 yr before the SN) and 28 (peak at  $\sim 300$  yr) of Ouchi & Maeda (2017) are shown for comparison, with model 28 (cyan) and model 25 shifted toward the SN by 5450 (blue) and 4300 (red) yr.

the late-time radio rebrightening with the timescale covering  $\sim 1$  yr to decades (Anderson et al. 2017; Chandra et al. 2020; Thomas et al. 2022); Margutti et al. (2017) showed that about 10% of SNe Ib/c exhibit radio (centimeter) rebrightening  $\sim 1$  yr after the explosion with typically an order of magnitude enhancement in the flux. It should be interesting to compare the characteristics of SN 2018ivc with those events, especially SN 2014C as the most well-studied example. Margutti et al. (2017) argued that the inner region is more like a cavity surrounded by an extremely dense CSM; an extremely high mass-loss rate ( $\sim 1 M_{\odot} \text{ yr}^{-1}$ )  $\sim 10$ – $1000$  yr before the explosion was followed by a mass loss consistent with a wind from a Wolf–Rayet star ( $\lesssim 10^{-5} M_{\odot} \text{ yr}^{-1}$  Smith 2017). Margutti et al. (2017) suggested as one possibility the scenario where the common envelope is responsible for the creation of the detached dense CSM, leaving a bare He star. The case for SN 2018ivc has two remarkable differences: (1) the initial, main mass loss ( $\sim 1500$  yr before the explosion) is less dramatic, and then (2) it keeps a relatively high mass-loss rate toward the explosion. Therefore, it fits better with the scenario proposed here (see also Ouchi & Maeda 2017; Maeda et al. 2023); the initial mass transfer was rapid but did not enter into the common envelope, and the rapid phase was over when the mass ratio was inverted. At that moment,  $\sim 1 M_{\odot}$  of the H-rich envelope was left, which kept filling the RL. An interesting alternative scenario may be a merger of the cores following the common envelope, in which the excited merger product may keep a high mass-loss rate up until the explosion (Nomoto et al. 1995, 1996).

Millimeter observations of SNe are extremely rare; therefore, virtually no samples are available to make any data-based estimate of the frequency of SNe showing rebrightening at millimeter wavelengths. Indeed, a well-defined control sample is still missing even at centimeter wavelengths (Bietenholz et al. 2021), which makes even a qualitative estimate of the frequency of rebrightening events somewhat fraught, with the possible exception of SNe Ib/c (see above; Margutti et al. 2017). Alternatively, we could estimate an expected rate of

such events based on the scenario proposed here (i.e., the boundary between the single and binary evolution channels). Maeda et al. (2023) gave such an estimate for the “SN 2018ivc-like” events based on the model sequence of Ouchi & Maeda (2017) as being  $\sim 10\%$  of SNe I Ib and  $\sim 3\%$ – $6\%$  of stripped-envelope supernovae (SESNe). This estimate indeed indicates that a nonnegligible fraction of SNe Ib/c showing rebrightening ( $\sim 10\%$  of SNe Ib/c; see above) may be linked to this binary evolution channel. On the other hand, the same fraction was estimated to be  $\sim 10\%$ – $20\%$  of SNe IIL, indicating that the evolutionary channel considered here is not a major channel toward SNe IIL, which might reflect potential “mixed populations” within SNe IIL (Arcavi et al. 2012; but see also Anderson et al. 2014). As compared to SNe IIP, SN 2018ivc-like events are very rare, with an expected rate of only  $\sim 3\%$  of SNe IIP (with large uncertainties), where we assume that the relative proportion of SNe IIP to SNe IIL is  $\sim 7:1$  (Li et al. 2011). These crude estimates suggest that the SN 2018ivc-like events, or the events linking the single and binary evolution channels, are intrinsically rare in the population of H-rich SNe. The SNe IIL would make especially interesting targets, as the above estimate suggests that the bulk of SNe IIL are unlikely to have originated in the specific binary evolutionary channel proposed here. A future sample of SNe IIL followed up in the radio, particularly at millimeter wavelengths, may reveal whether such rebrightening is exclusively associated with the SN 2018ivc-like objects.

Another possibility for the detached CSM is an external effect. For the detached CSM shell associated with SN 2014C, Milisavljevic et al. (2015) considered photoionization confinement of the CSM by an external radiation field imposed by neighboring stars in a stellar cluster based on the scenario proposed by Mackey et al. (2014). This scenario, however, is unlikely to work for SN 2018ivc; Bostroem et al. (2020) placed an upper limit of the MS mass of a progenitor star being  $\lesssim 11 M_{\odot}$  that existed at the SN location in pre-SN Hubble Space

Telescope images, even if it was a single star that existed at the SN location.

## 5. Concluding Remarks

We have presented long-term monitoring of the peculiar SN IIL 2018ivc ( $\sim 4$ –1364 days) with ALMA. It started showing rebrightening in its synchrotron flux  $\sim 300$ –500 days after the explosion. The radial CSM distribution as reconstructed from the long-term millimeter light curves shows a very high mass-loss rate exceeding  $10^{-3} M_{\odot} \text{ yr}^{-1} \sim 1500$  yr before the explosion, followed by a moderately high mass-loss rate of  $\gtrsim 10^{-4} M_{\odot} \text{ yr}^{-1}$  in the remaining evolution toward the SN explosion. This behavior is in line with the expectation from the scenario in which SN 2018ivc is indeed more like an “extended SN IIB” in its ejecta properties (i.e., a He star surrounded by  $\sim 1 M_{\odot}$  of the H-rich envelope) produced through the binary with a relatively large initial separation at a boundary between SNe IIB and SNe IIP (Ouchi & Maeda 2017; Maeda et al. 2023).







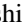
To our knowledge, it is the first example where rebrightening is detected in the millimeter synchrotron emission from SNe. Further, in the abovementioned scenario, it is the second example where the radio synchrotron rebrightening has been observed for an SN IIB. Indeed, SNe showing radio rebrightening are very rare. The comparison to the properties of the well-observed SN 2014C showing a transition from SN Ib to SN IIn shows that they likely share a similar (binary) evolution channel, albeit with some different details. It is likely that the strong binary interaction started at similar epochs ( $\sim 100$ –1000 yr before the explosion), while the outcome is different; SN 2018ivc is more likely explained by the rapid RL overflow (nonconservative) mass transfer leaving an RL-filling primary star, while SN 2014C entered into the common envelope and stripped away essentially all of the H-rich envelope. Identifying the cause of the difference is beyond the scope of the present work, but it may be due to, for example, the masses of the binary components (e.g., the mass ratio).

The models presented here suggest that  $\sim 1 M_{\odot}$  of the CSM has been swept up by day  $\sim 1500$ . As this is comparable to the expected envelope mass, the shock will start experiencing rapid deceleration afterward. Therefore, we predict that the synchrotron flux will shortly turn into the decay phase again. Further, if the mass budget for the CSM is  $\sim 5$ – $10 M_{\odot}$ , as expected in the binary evolution scenario for SNe IIB (and SESNe), we may assume that the characteristic shock velocity would be  $\sim 5000 \text{ km s}^{-1}$  after a substantial amount of this CSM is swept up. Given that there is additional CSM for another  $(0.5$ – $1) \times 10^{17} \text{ cm}$ , the shock will eventually break out of this CSM in 3–6 yr, after which the interaction will be essentially over. As such, we plan to continuously monitor SN 2018ivc, which could be done in part of the monitoring observations of NGC 1068. In addition, it could be an interesting target for continuous monitoring with very long baseline interferometry; we expect to start spatially resolving the shock expansion at  $\gtrsim 5$  yr for an angular resolution of  $\sim 0''.001$ . It could be an interesting target not only for existing facilities but also for future facilities such as the next-generation VLA (Murphy et al. 2018).

The authors thank the referee for constructive comments. This paper makes use of the following ALMA data: ADS/JAO. ALMA #2018.1.01135.S, #2018.1.01193.T, #2018.1.01506.S, #2018.1.01684.S, #2018.A.00038.S., #2019.1.00026.S,

and #2021.A.00026.S. Some of the ALMA data were retrieved from the JVO portal (<http://jvo.nao.ac.jp/portal/>) operated by ADC/NAOJ. ALMA is a partnership of ESO (representing its member states), NSF (USA) and NINS (Japan), together with NRC (Canada), MOST and ASIAA (Taiwan), and KASI (Republic of Korea), in cooperation with the Republic of Chile. The Joint ALMA Observatory is operated by ESO, AUI/NRAO and NAOJ. K.M. acknowledges support from Japan Society for the Promotion of Science (JSPS) KAKENHI grants JP18H05223, JP20H00174, and JP20H04737. K.M. was supported by the ALMA Japan Research Grant of the NAOJ ALMA Project, NAOJ-ALMA-269. T.M. appreciates the support from NAOJ ALMA Scientific Research grant No. 2021-17A. T.M. is supported by JSPS KAKENHI grant No. JP22K14073. H.K. was funded by Academy of Finland projects 324504 and 328898. M.I. acknowledges support from JSPS KAKENHI grant JP21K03632. The work is partly supported by the JSPS Open Partnership Bilateral Joint Research Projects between Japan and Finland (K.M. and H.K.; JPJSBP120229923).

## ORCID iDs

Keiichi Maeda  <https://orcid.org/0000-0003-2611-7269>  
 Tomonari Michiyama  <https://orcid.org/0000-0003-2475-7983>  
 Poonam Chandra  <https://orcid.org/0000-0002-0844-6563>  
 Stuart Ryder  <https://orcid.org/0000-0003-4501-8100>  
 Hanindyo Kuncarayakti  <https://orcid.org/0000-0002-1132-1366>  
 Daichi Hiramatsu  <https://orcid.org/0000-0002-1125-9187>  
 Masatoshi Imanishi  <https://orcid.org/0000-0001-6186-8792>

## References

- Anderson, G. E., Horesh, A., Mooley, K. P., et al. 2017, *MNRAS*, 466, 3648  
 Anderson, J. P., González-Gaitán, S., Hamuy, M., et al. 2014, *ApJ*, 786, 67  
 Arcavi, I., Gal-Yam, A., Cenko, S. B., et al. 2012, *ApJL*, 756, L30  
 Bauer, F. E., Dwarkadas, V. V., Brandt, W. N., et al. 2008, *ApJ*, 688, 1210  
 Bersten, M. C., Benvenuto, O. G., Nomoto, K., et al. 2012, *ApJ*, 757, 31  
 Bietenholz, M. F., Bartel, N., Argo, M., et al. 2021, *ApJ*, 908, 75  
 Bostroem, K. A., Valenti, S., Sand, D. J., et al. 2020, *ApJ*, 895, 31  
 Chandra, P., Chevalier, R. A., Chugai, N., Milisavljevic, D., & Fransson, C. 2020, *ApJ*, 902, 55  
 Chevalier, R. A. 1998, *ApJ*, 499, 810  
 Chevalier, R. A., & Fransson, C. 2006, *ApJ*, 651, 381  
 DeMarchi, L., Margutti, R., Dittman, J., et al. 2022, *ApJ*, 938, 84  
 Dessart, L., & Hillier, D. J. 2022, *A&A*, 660, L9  
 Fang, Q., Maeda, K., Kuncarayakti, H., Sun, F., & Gal-Yam, A. 2019, *NatAs*, 3, 434  
 Filippenko, A. V. 1997, *ARA&A*, 35, 309  
 Fremling, C., Ko, H., Dugas, A., et al. 2019, *ApJL*, 878, L5  
 Groh, J. H. 2014, *A&A*, 572, L11  
 Hamuy, M., Deng, J., Mazzali, P. A., et al. 2009, *ApJ*, 703, 1612  
 Hiramatsu, D., Howell, D. A., Moriya, T. J., et al. 2021, *ApJ*, 913, 55  
 Langer, N. 2012, *ARA&A*, 50, 107  
 Li, W., Leaman, J., Chornock, R., et al. 2011, *MNRAS*, 412, 1441  
 Mackey, J., Mohamed, S., Gvaramadze, V. V., et al. 2014, *Natur*, 512, 282  
 Maeda, K. 2012, *ApJ*, 758, 81  
 Maeda, K. 2022, Handbook of X-ray and Gamma-ray Astrophysics, ed. C. Bambi & A. Santangelo (Berlin: Springer), in press  
 Maeda, K., Chandra, P., Matsuoka, T., et al. 2021, *ApJ*, 918, 34  
 Maeda, K., Chandra, P., Moriya, T. J., et al. 2023, *ApJ*, 942, 17  
 Maeda, K., Hattori, T., Milisavljevic, D., et al. 2015, *ApJ*, 807, 35  
 Margutti, R., Kamble, A., Milisavljevic, D., et al. 2017, *ApJ*, 835, 140  
 Matheson, T., Filippenko, A. V., Ho, L. C., Barth, A. J., & Leonard, D. C. 2000, *AJ*, 120, 1499  
 Matsuoka, T., Maeda, K., Lee, S.-H., & Yasuda, H. 2019, *ApJ*, 885, 41  
 Milisavljevic, D., Margutti, R., Kamble, A., et al. 2015, *ApJ*, 815, 120

- Murphy, E. J., Bolatto, A., Chatterjee, S., et al. 2018, in ASP Conf. Ser. 517, Science with a Next Generation Very Large Array, ed. E. Murphy (San Francisco, CA: ASP), 3
- Mutic, I., Williams, D., Beswick, R., & Baki, P. 2022, ATel, 15521, 1
- Nomoto, K., Iwamoto, K., & Suzuki, T. 1995, PhR, 256, 173
- Nomoto, K., Iwamoto, K., Suzuki, T., et al. 1996, Compact Stars in Binaries, ed. J. van Paradijs, E. P. J. van den Heuvel, & E. Kuulkers, Vol. 165 (Dordrecht: Kluwer), 119
- Ouchi, R., & Maeda, K. 2017, ApJ, 840, 90
- Patat, F., Chugai, N., & Mazzali, P. A. 1995, A&A, 299, 715
- Ryder, S. D., Sadler, E. M., Subrahmanyan, R., et al. 2004, MNRAS, 349, 1093
- Shigeyama, T., Suzuki, T., Kumagai, S., et al. 1994, ApJ, 420, 341
- Smith, N. 2017, Handbook of Supernovae, ed. A. W. Alsabti & P. Murdin (Berlin: Springer), 403
- Soderberg, A. M., Chevalier, R. A., Kulkarni, S. R., & Frail, D. A. 2006, ApJ, 651, 1005
- Stroh, M. C., Terreran, G., Coppejans, D. L., et al. 2021, ApJL, 923, L24
- Tartaglia, L., Sand, D. J., Valenti, S., et al. 2018, ApJ, 853, 62
- THE CASA TEAM, Bean, B., Bhatnagar, S., et al. 2022, arXiv:2210.02276
- Thomas, B. P., Wheeler, J. C., Dwarkadas, V. V., et al. 2022, ApJ, 930, 57
- Tully, R. B., Rizzi, L., Shaya, E. J., et al. 2009, AJ, 138, 323
- Valenti, S., Sand, D. J., & Wyatt, S. 2018, TNSTR, 2018-1816, 1
- Woosley, S. E., Eastman, R. G., Weaver, T. A., & Pinto, P. A. 1994, ApJ, 429, 300
- Yoon, S.-C. 2017, MNRAS, 470, 3970